# Structural Modifications in Stretch-Induced Crystallization in PVDF Films as Measured by Small-Angle X-ray Scattering

**Dante Luis Chinaglia,[1] Rinaldo Gregório,Jr.,[2] Dimas Roberto Vollet[1]**

[1]*Unesp - Universidade Estadual Paulista, IGCE, Departamento de Física, Campus de Rio Claro*
[2]*UFSCar - Universidade Federal de São Carlos, Departamento de Engenharia de Materiais, Campus de São Carlos*

Received 5 July 2011; accepted 20 September 2011
DOI 10.1002/app.35684
Published online 22 December 2011 in Wiley Online Library (wileyonlinelibrary.com).

**ABSTRACT:** The nanostructure of stretched and nonstretched PVDF samples was studied by small-angle X-ray scattering (SAXS). The crystallinity of the samples was determined by wide-angle X-ray diffraction (WAXD) and differential scanning calorimetry (DSC), and crystalline phases by Fourier transform infrared spectroscopy (FTIR). The nanostructure can be described by a lamellar stacking of crystalline and amorphous layers, with a fairly well defined long period $D$ and a diffuse-boundary in the interface between the crystalline and amorphous phases. The crystallinity of the stretched sample was found to be greater than that of the nonstretched sample. The long period $D$ and the thicknesses of the crystalline lamellae $T_c$ were found to be greater in the stretched sample than those in the nonstretched sample. The thickness of the diffuse-boundary was evaluated as being $\sim$ 1.4 nm in the nonstretched sample and 1.1 nm in the stretched sample. It was concluded that the growth of the thickness of the crystalline layer induced by the stretching process (stretch-induced crystallization) occurs partially at expense of the diffuse boundary and also by the coarsening of the structure with the stretching process, because of the diminution in the surface area to volume ratio observed. © 2011 Wiley Periodicals, Inc. J Appl Polym Sci 125: 527–535, 2012

**Key words:** poly(vinylidene fluoride) (PVDF); crystalline-amorphous interface; SAXS; diffuse boundary; stretching

## INTRODUCTION

Poly(vinylidene fluoride), PVDF, is a semicrystalline polymer used in many technological applications due to its important pyroelectric and piezoelectric properties when polarized. PVDF can be crystallized into at least four different polymorphous structure, named α, β, γ, and δ. The structure of each one of these phases is well documented in the literature.[1] Wisniewski[2] employed the constant current technique[3] to determine the hysteresis loop and showed that the remnant polarization of β-PVDF has a stable and metastable component; the latter relaxes within $\sim$ 12 h after removal of the external electric field. Recently, it has been demonstrated[4,5] that drawing of PVDF films, in the α or in the β phases, increases the stable remnant polarization and reduces its metastable component.[4,5] Previous works demonstrated that stretching α-PVDF films also reduces the intensity of the dielectric relaxation $\alpha_c$.[6,7] This relaxation is observed by dielectric spectroscopy at low frequencies and attributed by several authors to the orientation of dipoles in the polymer crystalline region.[8–13] With base in those results, it was suggested that the metastable polarization, as well as, the dielectric relaxation $\alpha_c$ should be caused by dipolar orientation in the interfacial amorphous-crystalline region of the PVDF.[5] The existence of this interfacial region was firstly evidenced by Flory.[14] In the intermediated region, between the crystalline and amorphous phases, the polymer chains are less organized and not strongly linked as in the crystalline one. The dipoles contained in that interface have an intermediate mobility between that of crystalline and amorphous region. With stretching, those interface regions decrease and the crystalline region increases, reducing the metastable polarization and the dielectric relaxation $\alpha_c$ and increasing the stable remnant polarization of the PVDF; the latter being linked to the crystalline region of the polymer. However, until the present we have no knowledge of any work that has verified the influence of the stretching in the amorphous, in the interphase and crystalline regions of α-PVDF. The objective of the present work was to verify the nanostructural modifications α-PVDF caused by the stretching process using Small-Angle X-Ray Scattering (SAXS) technique.

*Correspondence to:* D. L. Chinaglia (dantelc@rc.unesp.br).
Contract grant sponsors: LNLS – National Synchrotron Light Laboratory, FAPESP, CNPq, INEO, nBioNet, Brazil.

## MATERIALS AND METHODS

### Sample preparation

PVDF films with thickness of 50 μm were purchased from Bemberg Folien GmbH. The non-stretched 50 μm films were used as-received and denominated sample A. A second sample were uniaxially drawn from the 50 μm films at a temperature of 130°C, draw ratio $R = 4$ and rate of 5 mm/min by using the device described in Ref. 15. This stretching condition was used because it practically does not cause the α→β phase transformation, and oriented α phase predominates.[16–18] The resulting films with thickness of ~ 12 μm were denominated sample B. In other to prepare the samples A and B for the SAXS experiment, small circular discs were cut and randomically joined to produce a thickness of 400 μm, which was estimated as the ideal attenuation for SAXS transmission experiment. An important result from this sample preparation methodology is that the film orientation was missed.

### Equipment

Fourier transform infrared spectroscopy (FTIR) spectra were obtained in Thermo Scientific model Nicolet iS10, in the wave number range between 400 and 1000 $cm^{-1}$ at a resolution of 2 $cm^{-1}$. Wide-angle X-ray diffraction (WAXD) analysis was carried out with a Rigaku Rotaflex (Mod. RU200B) diffractometer, operated at 40 kV and 80 mA with CuKα radiation (λ = 1.54 Å). Patterns were recorded in the 2θ range of 10–40°. The degree of crystallinity of samples A and B was determined by X-ray diffraction as a ratio of crystalline area to total area of the diffractogram. Differential scanning calorimetry (DSC) analyses were carried out using a Perkin–Elmer DSC-7, calibrated with In, in atmosphere of purified $N_2$ (10 mL/min) and heating rate of 10°C/min. The degree of crystallinity of samples was also determined by comparing the enthalpy of fusion of the sample obtained by DSC with that of 100% crystalline PVDF-α (104.5 J/g).[19] Small-Angle X-Ray Scattering (SAXS) experiments were carried out using synchrotron radiation with a wavelength λ = 0.1608 nm at the SAXS beam line of the LNLS synchrotron radiation facility, Campinas, Brazil. The beam was monochromatized by a silicon monochromator and collimated by a set of slits defining a pin-hole geometry. A 2D position-sensitive x-ray detector was used to obtain SAXS intensity from isotropic systems as a function of the modulus of the scattering vector $q = (4\pi/\lambda)\sin(\varepsilon/2)$, where ε = 2θ is the scattering angle. The experimental setup allowed us to obtain SAXS data from $q_0 = 0.069$ $nm^{-1}$ up to $q_m = 1.68$ $nm^{-1}$ in intervals of $q = 6.52 \times 10^{-3}$ $nm^{-1}$. The data were corrected by sample attenuation and parasitic scattering, and normalized with respect to the beam intensity.

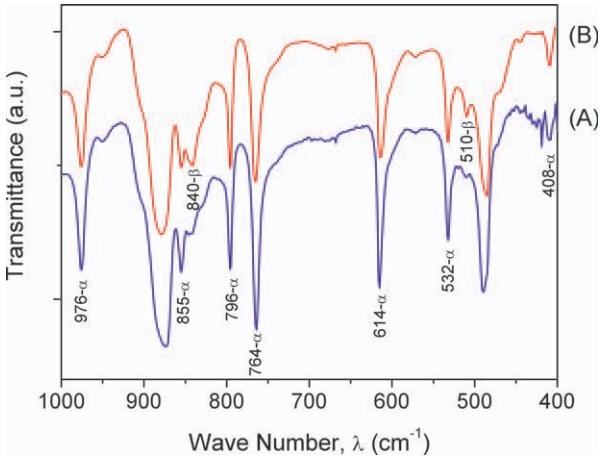


**Figure 1** FTIR spectra of samples A and B. The characteristic absorption bands of the α and β phase are indicated in the figure. [Color figure can be viewed in the online issue, which is available at wileyonlinelibrary.com.]

## RESULTS AND DISCUSSION

### Sample characterization

Samples were characterized by means of FTIR to verify the crystalline phase(s) present. Spectra are shown in Figure 1.

It can be seen that sample A contains predominantly the α phase, evidenced by the characteristic bands of this phase: 408, 532, 614, 764, 796, 855, and 976 $cm^{-1}$.[20,21] After drawing (Sample B) weak bands appeared at 510 and 840 $cm^{-1}$ characteristic of the β phase.[20,21] Thus, drawing carried out at 130°C with $R = 4$ has little effect on the crystalline phase of the sample, as observed in previous works.[16–18] Under these conditions the *c*-axis of the crystalline chains is preferentially oriented parallel to drawing with minor α→β transformation, as shown in a previous work.[16]

Samples A and B were also submitted to X-ray diffraction (WAXD) and the diffractograms are shown in Figure 2. Both samples displayed strong peaks at 2θ = 17.8, 18.4, and 20.1 attributed to the diffractions in the (100), (020), and (110) planes, respectively, all characteristic of the α phase.[22] The weak peaks at 25.6, 36.0, and 37.2 attributed to the diffractions in the (120), (200), and (210)/(040) planes respectively are also characteristic of the α phase.[22] The difference between the intensities of the peaks corresponding to each plane for the two samples is due to the increase in crystallite orientation and degree of crystallinity, both caused by drawing. These results confirm those obtained by FTIR. The degree of crystallinity, or the volume fraction of the

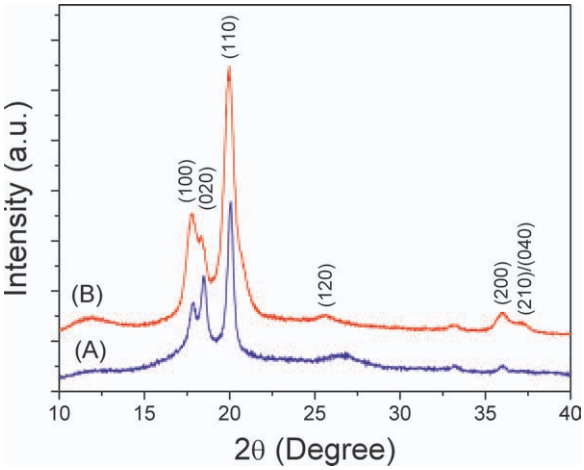


**Figure 2** WAXD spectra of samples A and B. [Color figure can be viewed in the online issue, which is available at wileyonlinelibrary.com.]

crystalline phase $\phi_c$, of samples A and B evaluated by X-ray diffraction was 47 and 62%, respectively.

The mass fraction of the crystalline phase $\phi_m$ of the samples A and B evaluated by DSC was 53 and 58%, respectively, which correspond to the volume fraction of the crystalline phase $\phi_c$ equal to 49 and 54%, if we use the relationship $\phi_c = \phi_m(\rho/\rho_c)$, where $\rho$ is the PVDF density (1.78 g/cm$^3$) and $\rho_c$ is the crystalline $\alpha$-phase density (1.92 g/cm$^3$).

Table I resumes the values for the crystallinity $\phi_c$ of the samples A and B as obtained by WAXD and DSC.

### Small-angle X-ray scattering

#### Bragg's law

Figure 3(I) shows SAXS patterns for stretched (B) and nonstretched (A) PVDF samples. The SAXS profiles exhibit a very intense scattering peak associated to the crystalline-amorphous structure of the partially crystalline PVDF.

The data were analyzed in terms of a one-dimensional stack model, the stacks consisting of crystalline lamellae separated by amorphous layers. The correlation function of the electron density heterogeneities for a single stack of the ideal lamellar model varies in one direction only, let $x$. If $\gamma_1(x)$ is the value of the correlation function in the $x$-direction then it could be obtained by Fourier transformation of the one-dimensional intensity function given by $I_1(q) = q^2I(q)$, where $I(q)$ is the isotropic three-dimensional intensity function. The transformation $I_1(q) = q^2I(q)$ is known as Lorentz-correction.[23] The peak (or peaks) in the one-dimensional intensity function $I_1(q)$ can be assigned to the Bragg reflection from the lamellae, so the average value of the long period $D$, which is the sum of average thicknesses of the crystalline layers $T_c$ and the amorphous layers $T_a$, can be obtained from Bragg's law as[23]

$$D = 2\pi/q^*, \tag{1}$$

where $q^*$ is the position of the first order Bragg peak in the $q$-space.

Figure 3(II) shows the plots of $q^2I(q)$ versus $q$ for the stretched (B) and non-stretched (A) PVDF samples. The Bragg peak appears at $q^* = 0.535$ nm$^{-1}$ for the stretched sample and at $q^* = 0.626$ nm$^{-1}$ for the nonstretched sample. The peak was found broader in the nonstretched sample. Table II shows the average values for the long period $D$ together with $T_c$

**TABLE I**
**The Volume Fraction of the Crystalline Phase $\phi_c$ of the PVDF Samples as Determined by WAXD and DSC**

| Sample | $\phi_c$ (WAXD) | $\phi_c$ (DSC) | $\phi_c$ (Mean value) |
|---|---|---|---|
| A | 0.47 | 0.49 | 0.48 |
| B | 0.62 | 0.54 | 0.58 |

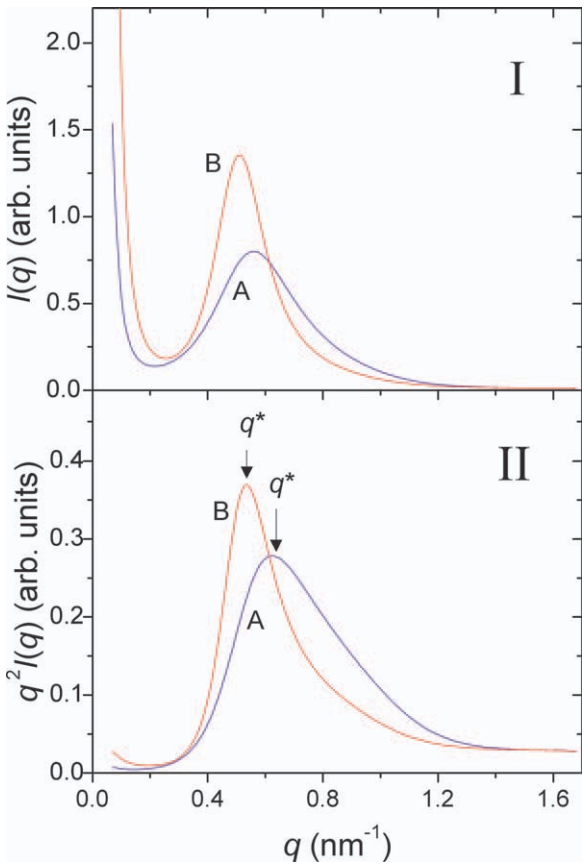


**Figure 3** (I) SAXS intensities for stretched (B) and non-stretched (A) PVDF samples. (II) The Lorentz transformation for obtaining the one-dimensional intensity $I_1(q) = q^2I(q)$ characteristic of lamellar systems. [Color figure can be viewed in the online issue, which is available at wileyonlinelibrary.com.]

**TABLE II**
**Average Value for the Long Period $D$ Determined from the SAXS Peak and the Values for the Thicknesses of the Crystalline Layers $T_c$ and the Amorphous Layers $T_a$ Evaluated from the Mean Value for $\phi_c$ in Table I**

| Sample | $D$ (nm) | $T_c = \phi_c D$ (nm) | $T_a = (1 - \phi_c)D$ (nm) |
|---|---|---|---|
| A | 10.0 | 4.8 | 5.2 |
| B | 11.7 | 6.8 | 4.9 |

and $T_a$ as evaluated through $T_c = \phi_c D$ and $T_a = (1 - \phi_c)D$ by using the mean value for $\phi_c$ in Table I.

Porod's law

The scattering intensity $I(q)$ at high-$q$ from a two-phase structure with sharp phase boundaries, each phase occupying respectively the fractions $\phi_c$ and $(1 - \phi_c)$ of the sample volume $V$, is given by[23]

$$\lim_{q\to\infty} q^4 I(q) = K_p = (S/V)Q/\pi\phi_c(1 - \phi_c) \qquad (2)$$

where $K_p$ is a constant, known as constant of Porod's law, $S$ is the surface area of the interface between the phases, so $(S/V)$ represents the surface to volume ratio, and $Q$ is the invariant given by

$$Q = \int_0^\infty q^2 I(q) dq \qquad (3)$$

Porod's law should be observed at high-$q$ for sharp phase boundaries since $q > 1/T$, where $T$ is the minimal thickness of the phases, which means $T_c$ and $T_a$ for the case of the PVDF lamellar structure.

Positive deviations from Porod's law should occur when the phases present fluctuations in the electron densities in a molecular level. In polymeric materials, fluctuations are often three-dimensional and the contribution to the scattering is a constant value $I_b$ independent of $q$. In this case, the Porod law can be written as.[24]

$$\lim_{q\to\infty} q^4 I(q) = K_p + I_b q^4 \qquad (4)$$

Figure 4 shows the plots of $q^4 I(q)$ versus $q^4$ to probe Porod's law at high-$q$ for the PVDF samples. The samples obey reasonable well the eq. (4) at high-$q$. The parameters $K_p$ and $Q$ are shown in Table III together with other evaluated structural parameters. For the obtaining of $Q$, the background $I_b$ has been subtracted from measured intensity $I(q)$ and the integration of eq. (3) above $q = q_m = 1.68$ nm$^{-1}$ (the maximum value of $q$ experimentally accessible in this available setup) up to the infinity was obtained by $K_p/q_m$. The surface to volume ratio $(S/V)$ was obtained from eq. (2) by using the mean value for $\phi_c$ in Table I.

For a perfectly lamellar structure, we should have $(S/V) = 2/D$, so $D = 2(V/S)$ and the average thicknesses of the crystalline layers $T_c$ and the amorphous layers $T_a$ could be evaluated by $T_c = \phi_c D$ and $T_a = (1\text{-}\phi_c)D$, since $D = T_c + T_a$. Table III shows that the values of such structural parameters evaluated from Porod's law are in reasonable agreement with the corresponding values obtained from the Bragg peak (Table II), but the values from Porod's law are even lower than those obtained from the Bragg peak. This occurs because there is an interface distribution function so the surface to volume ratio $(S/V)$ obtained from Porod's law is more weighted by the minor distances in the interface distribution function.

Interface distribution function

It has been well established the concept of the interface distribution in lamellar structures.[23,25–28] The interface distribution function is obtained from the second derivative $\gamma_1''(x)$ of the one-direction correlation function $\gamma_1(x)$. The correlation function in the $x$-direction is obtained by Fourier transformation of the one-dimensional intensity function given by

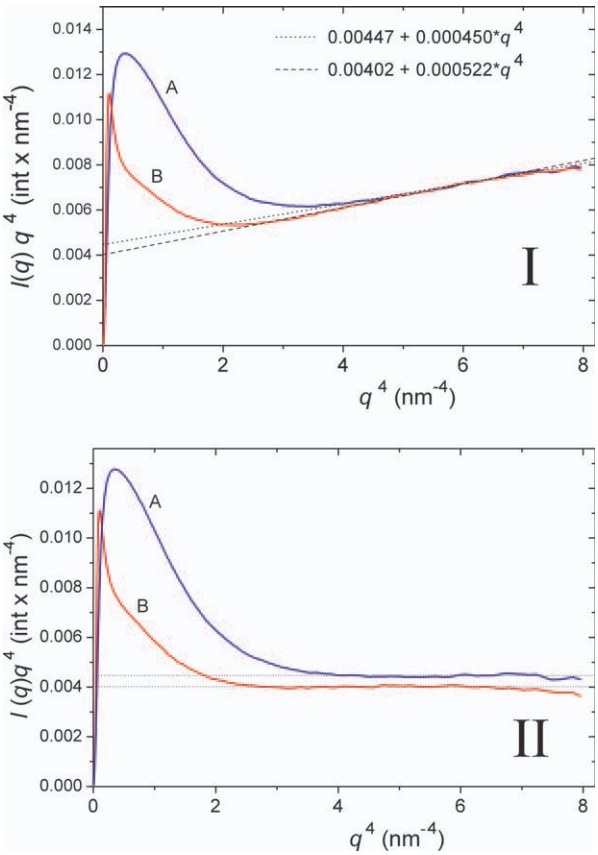


**Figure 4** (I) Plots of Porod's law for the PVDF samples with the fitting of eq. (4). (II) Plots after the background subtraction $[I(q) - I_b]$. [Color figure can be viewed in the online issue, which is available at wileyonlinelibrary.com.]

**TABLE III**
**Structural Parameters Obtained from Porod's Law for the PVDF Samples**

| Sample | $K_p$ (Int×nm$^{-4}$) | $Q$ (Int×nm$^{-3}$) | $S/V$ (nm$^{-1}$) | $D = 2(V/S)$ (nm) | $T_c = \phi_c D$ (nm) | $T_a = (1 - \phi_c)D$ (nm) |
|---|---|---|---|---|---|---|
| A | 0.00447 | 0.0171 | 0.205 | 9.8 | 4.7 | 5.1 |
| B | 0.00402 | 0.0159 | 0.193 | 10.4 | 6.0 | 4.4 |

The values for $(S/V)$ and for the thicknesses of the crystalline layers $T_c$ and the amorphous layers $T_a$ were evaluated from the mean value of $\phi_c$ in Table I.

$I_1(q) = q^2 I(q)$, where $I(q)$ is the isotropic three-dimensional intensity function. Then,

$$\gamma_1(x) = (1/Q)\int_0^\infty q^2 I(q)\cos(qx)dq \quad (5)$$

and

$$\gamma_1''(x) = -(1/Q)\int_0^\infty q^4 I(q)\cos(qx)dq \quad (6)$$

Equation 6 represents the Fourier transform of $q^4 I(q)$. The part of the integration of eq. (6) at $q \to \infty$, corresponding to Porod's law $q^4 I(q) = K_p$, can be separated leading to a δ-function at the origin of $\gamma_1(x)$, which can be neglected in the calculation of $\gamma_1(x)$.[23,25] Then, the interface distribution function (IDF) can be obtained by[23]:

$$\gamma_1''(x) = (1/Q)\int_0^\infty [K_p - q^4 I(q)]\cos(qx)dq \quad (7)$$

Figure 5 shows the interface distribution function (IDF) for the PVDF samples calculated through eq. (7) from the SAXS intensity $I(q)$ after the subtraction of the background $I_b$ and using the Porod's law constant $K_p$ of Table III.

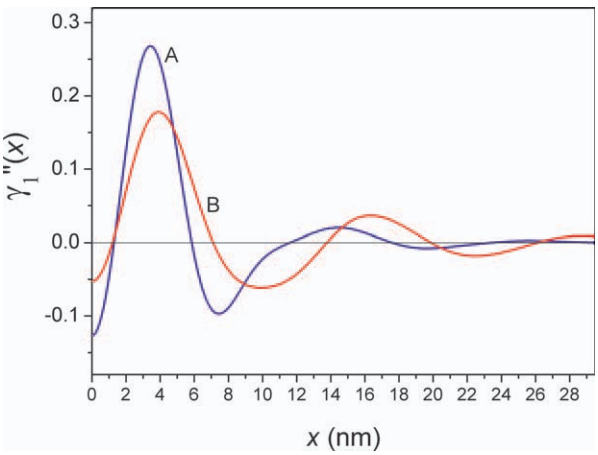


**Figure 5** Interface distribution function for the PVDF samples (A and B) as obtained from the SAXS intensity $I(q)$ after the subtraction of the background $I_b$. [Color figure can be viewed in the online issue, which is available at wileyonlinelibrary.com.]

We paid particular attention in the parameter $\gamma_1''(0)$, which was found to be clearly negative in the IDF curves for the PVDF samples of Figure 5; $\gamma_1''(0)$ was found to be more negative in the nonstretched (A) sample than that in the stretched (B) one. Expanding $\gamma_1(x)$ in the vicinity of $x \to 0$ up to the second order term, we would have

$$\gamma_1(x) = \gamma_1(0) + \gamma_1'(0)x + (1/2)\gamma_1''(0)x^2. \quad (8)$$

The term $\gamma_1(0)$ is naturally equal to 1 by equation 5. The second $\gamma_1'(0)$ is negative accounting for the decrease of $\gamma_1(x)$ with $x$ in the vicinity of $x \to 0$. It gives the surface to volume ratio $(S/V)$ of the lamellar system in the case of phases with sharp interface boundaries through the equation[23]:

$$\gamma_1'(0) = -(S/V)/2\phi_c(1 - \phi_c). \quad (9)$$

The thirst term $\gamma_1''(0)$ in equation 8, being negative, would account for diffuse boundaries of the interface between the phases. Formally, $\gamma_1''(0)$ is related to the amount of neighboring interfaces with zero distance, so it should be zero, or at least close to zero, in the case of a one-dimensional stack of laterally extended lamellae with sharp phase boundaries.[27] From equation 7, $\gamma_1''(0)$ can be cast as

$$\gamma_1''(0) = (1/Q)\int_0^\infty [K_p - q^4 I(q)]dq. \quad (10)$$

Since the integration of eq. (10) has resulted in negative values for the PVDF samples (the values of IDF curves at the origin in Fig. 5), we infer that there should be a diffuse boundary in the system, which has been likely masked by the background $I_b$, and which would be able to render eq. (10) to zero in the case of the intensity be appropriately corrected by such a diffuse boundary contribution.

We assumed a sigmoidal-gradient model defined by a Gaussian smoothing function given by $\exp(-\sigma^2 q^2)$ for such a diffuse boundary correction, where σ is a measure of the thickness of the diffuse boundary.[29] Since the contribution of the diffuse

**TABLE IV**
**Diffuse Boundary Thickness Estimated for the PVDF Samples**

| Sample | σ (nm) | $L_I \approx 2\sigma$ (nm) |
|---|---|---|
| A | 0.68 | 1.36 |
| B | 0.53 | 1.06 |

boundary to the intensity should be anyway corrected for the calculation of the interface distribution function (IDF), then, above a certain value $q_p$ of the measured high-$q$ region, the corrected quantity $q^4I(q)$ should match with the Porod law constant $K_p$. Then the correction by the diffuse boundary is only necessary to be carried out up to $q_p$, since the corrected $q^4I(q)$ is equal to $K_p$ for $q > q_p$. These coupled conditions can be synthesized as

$$K_p - q_p^4 I(q_p) \exp(-\sigma^2 q_p^2) = 0 \tag{11}$$

and

$$\int_0^{q_p} [K_p - q^4 I(q) \exp(-\sigma^2 q^2)] dq = 0. \tag{12}$$

Equations (11) and (12) were solved numerically for $q_p$ and σ for the PVDF samples. The thickness $L_I$ of diffuse boundary was assumed as being $\sim 2\sigma$[29,30] and the values are shown in Table IV. The thickness of the diffuse boundary in the nonstretched (A) sample was found to be about 30% larger than that of the stretched (B) sample, suggesting that the stretching process diminishes the thickness of the diffuse interface boundary.

Figure 6 shows the interface distribution function (IDF) for the PVDF samples after the additional correction by the diffuse boundary contribution. The fundamental assumption of such a model is that the thickness of the crystalline lamella and amorphous layers vary independently and are described by independent distribution functions $P_c(x)$ and $P_a(x)$.[25] These independent thickness distribution functions produce two positive peaks in the IDF function, where the first maximum can be assigned to the average thickness of the crystalline lamella $T_c$ and the second to the thickness of the amorphous layers $T_a$, when $\phi_c < 0.5$, and vice-versa when $\phi_c > 0.5$.[23] In the case of $\phi_c$ not to be much different from 0.5, the separation of the peaks is difficult as seem to be the case of the IDF curves in Figure 6. The first negative peak in the IDF curve is assigned to the long period distribution $P_D(x)$ which is result of the convolution of the distribution functions $P_c(x)$ and $P_a(x)$.[23] The minimum of the $P_D(x)$ distribution gives the average long period $D$ of the lamellar structure. The long period $D$ obtained from the minima in the IDF curves in Figure 6 was found to be about 8.2 nm for the nonstretched (A) PVDF and about 9.8 nm for the stretched (B) sample. These values are even lower than those obtained from Porod's law (Table III) without either correction by the diffuse boundary.

Since $P_c(x)$ and $P_a(x)$ were found not to be well resolved in the first positive peak of the IDF curves of Figure 6, a direct determination of $T_c$ and $T_a$, and therefore $\phi_c$, cannot be obtained with precision. However, we could get some estimative for these parameters by making some assumptions. We assumed that the thickness distribution functions $P_c(x)$ and $P_a(x)$ are normalized Gaussian centered at the average thicknesses $T_c$ and $T_a$ with standard deviations $w_c$ and $w_a$, respectively.[25] Then

$$P_c(x) = [1/w_c(2\pi)^{1/2}] \exp[-(x - T_c)^2/2w_c^2] \tag{13}$$

and

$$P_a(x) = [1/w_a(2\pi)^{1/2}] \exp[-(x - T_a)^2/2w_a^2], \tag{14}$$

and, since $P_D$ is the convolution between $P_c(x)$ and $P_a(x)$,

$$P_D(x) = [1/(w_c^2 + w_a^2)^{1/2}(2\pi)^{1/2}] \times \exp\{-[x - (T_c + T_a)]^2/2(w_c^2 + w_a^2)\}. \tag{15}$$

The set of eqs. (13)–(15) has only four independent parameters, which are $T_c$, $T_a$, $w_c$, and $w_a$, or $\phi_c$, $D$, $w_c$, and $w_a$, since $\phi_c = T_c/D$ and $D = T_a + T_c$.

The experimental IDF curves in Figure 6 were then fitted by the sum $P_c(x) + P_a(x) - P_D(x)$, with an approximately common factor for the sum, to obtain the parameters $\phi_c$, $D$, $w_c$, and $w_a$. Figure 7 shows the

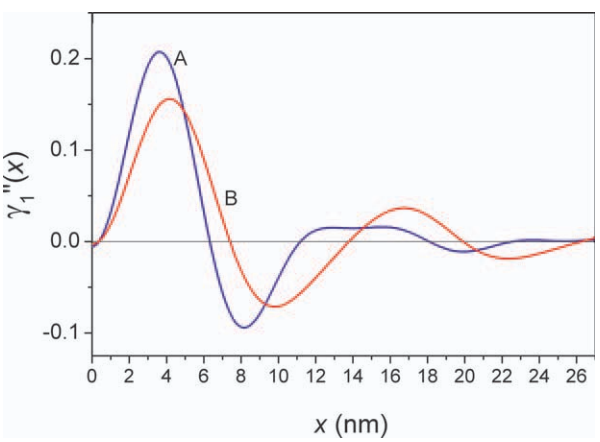


**Figure 6** Interface distribution function (IDF) for the PVDF samples after the additional correction by the diffuse-boundary contribution. [Color figure can be viewed in the online issue, which is available at wileyonlinelibrary.com.]

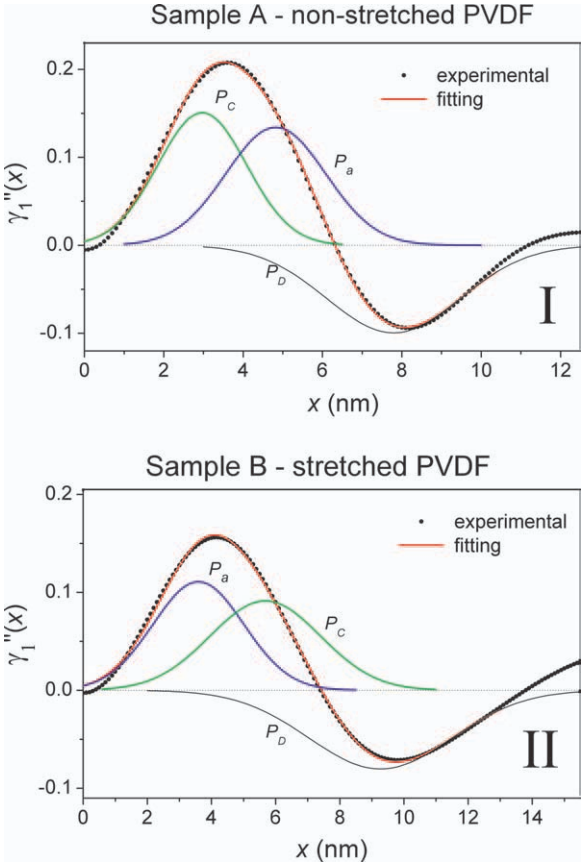


**Figure 7** Fitting the experimental IDF curves by normal Gaussian distributions for the thickness of the crystalline lamella $P_c(x)$, (I), and amorphous layers $P_a(x)$ and their convolution $P_D(x)$, (II). [Color figure can be viewed in the online issue, which is available at wileyonlinelibrary.com.]

fitting process and Table V the fitted parameters together with other structural parameters evaluated.

The distances associated to the structural parameters in Table V are in the general smaller than those corresponding in Table III, which were obtained from Porod's law with $\phi_c$ given by the mean value of Table I, without any correction by the diffuse boundary. Particularly, the value $\phi_c = 0.61$ for the stretched (B) PVDF in Table V is in agreement with the value from WAXD but the value $\phi_c = 0.38$ for the nonstretched (A) sample is very smaller than those given by either WAXD or DSC.

The discrepancies in the distances evaluated from IDF curves (Table V) with respect to those evaluated from Porod's law (Table III) could be explained by analyzing more carefully the effect of the diffuse boundary correction employed in this study. Because of the diffuse boundary to be masked by the background contribution at high-$q$, we only could correct the intensity up to a not-so-high value of $q$, in order to match the conditions stated by eqs. (11) and (12), but we had no means to correct also the value of the Porod law constant $K_p$, which value could be lower than that given in Table III. A lower value for $K_p$ certainly yield larger distances associated to the structural parameters determined from the IDF curves. We have no sure way to resolve such a possible diminution in $K_p$ because of the impossibility to separate completely the background from the diffuse-boundary effect at high-$q$ in the present data. However, a first approximation for the true distances could be obtained by adding an appropriate function of the diffuse-boundary thickness $L_I$ to the distances obtained from the IDF curves corrected by the diffuse-boundary. A reasonable approximation for such a correction could be $T_c' = T_c$

**TABLE V**
**Structural Parameters Determined by Fitting the IDF Curves by Normal Gaussian Distributions for the Thicknesses of Crystalline Lamella and Amorphous Layers**

| Sample | $\phi_c$ | $D$ (nm) | $w_c$ (nm) | $w_a$ (nm) | $T_c$ (nm) | $T_a$ (nm) |
|---|---|---|---|---|---|---|
| A | 0.38 | 7.8 | 1.1 | 1.7 | 3.0 | 4.8 |
| B | 0.61 | 9.3 | 1.7 | 1.4 | 5.7 | 3.6 |

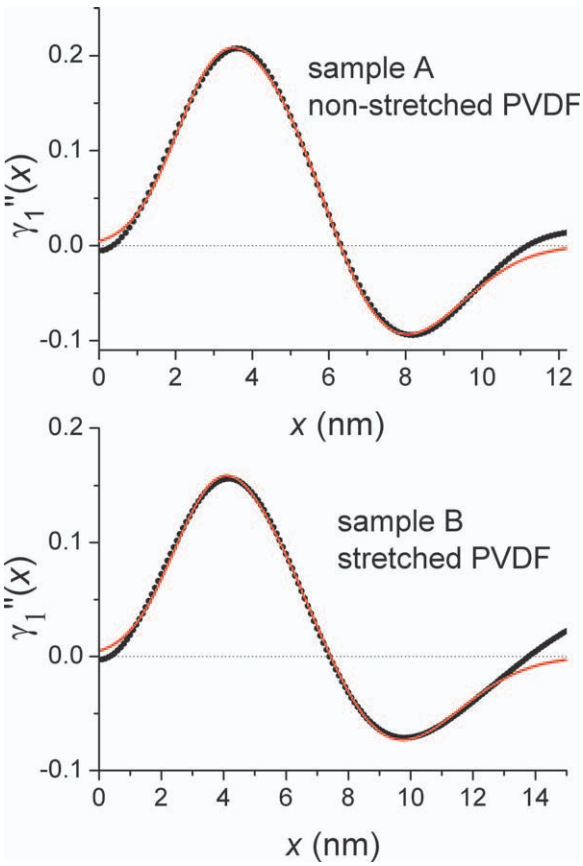


**Figure 8** Fitting of eqs. (13)–(15) to the experimental IDF curves (points) using the transformation $T_c = T_c' - L_I$, $T_a = T_a' - L_I$, and $D = D' - 2L_I$ to account for a reasonable diffuse-boundary correction. [Color figure can be viewed in the online issue, which is available at wileyonlinelibrary.com.]

**TABLE VI**
**Structural Parameters Evaluated Using the Transformation: $T_c = T_c' - L_I$, $T_a = T_a' - L_I$, and $D = D' - 2L_I$ to fit the IDF curves through eqs. (13)–(15)**

| Sample | $D'$ (nm) | $T_c'$ (nm) | $T_a'$ (nm) | $\phi_c'$ |
|---|---|---|---|---|
| A | 9.9 | 4.0 | 5.9 | 0.41 |
| B | 12.0 | 7.1 | 5.0 | 0.59 |

$+ L_I$, $T_a' = T_a + L_I$, $D' = D + 2L_I$, and $\phi_c' = (T_c + L_I)/(D + 2L_I)$.

Then the IDF curves were fitted again by eqs. (13)–(15) solving for the corrected thicknesses $T_c'$ and $T_a'$, and the long period $D'$, using the transformation $T_c = T_c' - L_I$, $T_a = T_a' - L_I$, and $D = D' - 2L_I$. Figure 8 shows that this transformation yields a completely equivalent fitting to the IDF curves with practically the same values for $w_c$, $w_a$, and for the amplitudes, but with $T_c'$, $T_a'$, $D'$, and $\phi_c' = T_c'/D'$ given in Table VI.

The results obtained for the distances $T_c'$, $T_a'$, $D'$ are in better agreement with those presented in Tables II and III, when compared with those in Table V. The values of the crystallinity $\phi_c'$ are even in a better agreement with the corresponding mean values of Table II, when compared with those in Table V. However, the value $\phi_c' = 0.41$ obtained for the nonstretched (A) PVDF is still smaller than either of the values from DSC or WAXD. This suggests that the crystallinity for the nonstretched sample could really be smaller than that generally obtained by others techniques.

## CONCLUSIONS

The structure of stretched and nonstretched PVDF samples can be described by a lamellar stacking of crystalline and amorphous layers, with a fairly well defined long period $D$ and a diffuse-boundary in the interface between the crystalline and amorphous phases.

The mean values for the thicknesses of the crystalline lamellae $T_c$ and the amorphous layers $T_a$, as evaluated from different methods employed in this study, were found to be $T_c = 4.4$ nm and $T_a = 5.5$ nm, for the nonstretched sample, and $T_c = 6.6$ nm and $T_a = 4.8$ nm, for the stretched sample, which correspond to the mean values $D = 9.9$ nm and 11.4 nm for the long period of the nonstretched and the stretched sample.

The thickness of the diffuse-boundary was evaluated as being $\sim 2\sigma = 1.4$ nm for the nonstretched sample and $2\sigma = 1.1$ nm for the stretched sample if we assume a sigmoidal-gradient model given by Gaussian smoothing function with standard deviation $\sigma$ for the diffuse boundary. Therefore, in fact drawing $\alpha$-PVDF films at 130°C and a draw ratio of 4 increases crystallinity and reduces the crystal-amorphous interphase region, as suggested in previous work.[5]

This set of results suggests that the growth of the thickness of the crystalline layer induced by the stretching process (stretch-induced crystallization) occurs partially at expense of the diffuse boundary, but also by the coarsening of the structure in the stretching direction because of the diminution of the surface area to volume ratio observed. We think the drawing process stretches mainly the amorphous region in a first stage, forcing mechanically the alignment of the polymer chains gradually in the diffuse boundary, which facilities the subsequent crystallization by temperature activation.

We should emphasize that this paper presents an original method to probe the diffuse boundary thickness in lamellar polymeric structures which could be very useful to study similar systems.

## References


1. Tashiro, K. In Ferroelectric Polymers; Nalwa, H. S., Ed.; Marcel Dekker: New York, 1995; p 63.
2. Wisniewski, C. Caracterização de polímeros ferroelétricos: metodologia e resultados, PhD thesis, University of São Paulo – USP, São Carlos, SP, Brazil, 1999.
3. Wisniewski, C.; Ferreira, G. F. L.; Moura, W. A.; Giacometti, J. A. J Phys D Appl Phys 2000, 33, 2483.
4. Silva, A. B.; Wisniewski, C.; Esteves, J. V. A.; Gregorio, R., Jr. J Mater Sci 2010, 45, 4206.
5. Silva, A. B.; Wisniewski, C.; Esteves, J. V. A; Gregorio, R., Jr. Ferroelectrics 2011, 413, 220.
6. Singh, R.; Kumar, J.; Singh, R. K.; Kaur, A.; Sinhá, R. D. P.; Gupta, N. P. Polymer 2006, 47, 5919.
7. Ozkazanc, E.; Guney, H. Y.; Oskay, T.; Tarcan, E. J Appl Polym Sci 2008, 109, 3878.
8. Mijovic, J.; Sy, J. W.; Kwei, T. K. Macromolecules 1997, 30, 3042.
9. Nakagawa, K.; Ishida, Y. J Polym Sci Polym Phys Ed 1973, 11, 1503.
10. Yano, S.; Tadano, K.; Aoki, K. J Polym Sci Polym Phys Ed 1974, 12, 1875.
11. Chanmal, C. V.; Jog, J. P. Exp Polym Let 2008, 2, 294.
12. Singh, R.; Kumar, J.; Singh, R. K.; Kaur, A.; Sinhá, R. D. P.; Gupta, N. P. Polymer 2006, 47, 5919.
13. Ozkazanc, E.; Guney, H. Y.; Oskay, T.; Tarcan, E. J Appl Polym Sci 2008, 109, 3878.
14. Flory, P. J. J Chem Phys 1949, 17, 223.
15. Constantino, C. J. L.; Job, A. E.; Simões, R. D.; Giacometti, J. A.; Zucolotto, V.; Oliveira, O. N., Jr.; Gozzi, G.; Chinaglia, D. L. Appl Spectr 2005, 59, N 3, 275.
16. Branciforti, M. C.; Sencadas, V.; Lanceros-Mendez, S.; Gregorio, R., Jr. J Polym Sci Part B Polym Phys 2007, 45, 2793.
17. McGrath, J. C.; Ward, I. M. Polymer 1980, 21, 855.
18. Hsu, T. C.; Geil, P. H. J Mater Sci 1989, 24, 1219.
19. Nakagawa, K.; Ishida, Y. J Polym Sci Polym Phys 1973, 11, 2153.
20. Kobayashi, M.; Tashiro, K.; Tadokoro, H. Macromolecules 1975, 8, 158.
21. Gregorio, R., Jr. J Appl Polym Sci 2006, 100, 3272.

22. Davis, G. T.; McKinney, J. E.; Broadhurst, M. G.; Roth, S. C. J Appl Phys 1978, 49, 4998.
23. Glatter, O.; Kratky, O.; Small Angle X-Ray Scattering; Academic Press: London, 1982.
24. Ruland, W. J Appl Cryst 1971, 4, 70.
25. Stribeck, N.; Ruland, W. J Appl Cryst 1978, 11, 535.
26. Ruland, W. Coll Polym Sci 1977, 255, 417.
27. Albrecht, T.; Strobl, G. Macromolecules 1995, 28, 5827.
28. Denchev, Z.; Nogales, A.; Ezquerra, T. A.; Fernandes-Nascimento, J.; Baltà-Calleja, F. J. J Polym Sci Part B: Polym Phys 2000, 38, 1167.
29. Koberstein, J. T.; Morra, B.; Stein, R. S. J Appl Cryst 1980, 13, 34.
30. Bonk, F. A.; Caldarelli, S.; Phan, T.; Bertin, D.; DeAzevedo, E. R.; Mantovani, G. L.; Bonagamba, T. J.; Plivelic, T. S.; Torriani, I. L. J Polym Sci B Polym Phys 2010, 48, 55.